A Decentralized Control Strategy Based on V-I Droop for Enhancing Dynamics of Autonomous Hybrid AC/DC Microgrids

Mohammad S. Golsorkhi and Mehdi Savaghebi, *Senior Member, IEEE*

***Abstract*—This article presents a GPS-based decentralized control strategy for hybrid ac/dc microgrids. The proposed method uses V-I droop characteristics for the distributed energy resources (DERs) in each of ac and dc subgrids. In particular, the output voltage of each DER is adjusted as a piecewise linear function of the per-unit (pu) output current. In addition, a droop control method is proposed for the interlink converter (IC) to attain global power sharing among the dc and ac DERs. The IC controller changes the deviation of the ac bus voltage as a function of the deviation of the dc bus voltage. This way, the power flow between ac and dc subgrids is adjusted such that the ac and dc DERs experience the same pu voltage deviation and hence deliver the same pu current and active power. In contrast with the existing control approaches, the proposed method does not require frequency or power calculations but directly uses voltage and current measurements in the control loops. So the delay associated with the feedback signals is minimized, which avails accurate load sharing during transients. Experimental results show the proposed method eliminates the transient overshoots of DERs' output powers by offering a fast and overdamped dynamic response.**

***Index Terms*—Dispersed storage and generation, droop control, microgrids (MG), inverters, power control, power electronics.**

I. Introduction

THE hybrid ac/dc microgrid (HMG) has become an established concept for the integration of dc and ac distributed energy resources (DERs) and loads [1]. An HMG is comprised of a dc microgrid (MG) and an ac MG. The dc MG enables the connection of dc sources (e.g., photovoltaic, fuel cell) and dc loads (e.g., LED lights, electric vehicles) without using of dc/ac and ac/dc conversion stages, which are necessary in pure ac MGs [2]. The ac MG facilitates integrating ac DERs in the grid and supplying ac loads. The dc and ac MGs are connected through a bidirectional dc/ac and ac/dc converter, referred to as interlink converter (IC). This way, active power can be the transferred from dc to ac subgrid and vice-versa to enable coordination of dc and ac DERs. Furthermore, the IC can participate in supplying the reactive power of the ac load. The HMG might be connected to the main power grid or be operated in islanded mode. This article is focused on the islanded operation mode, where the HMG relies on coordinated control of DERs for power balancing and voltage/frequency control.

Over the past couple of decades, numerous control methods have been proposed for pure dc and pure ac MGs. A widely accepted control method for ac MGs is the active power-frequency (P-f) and reactive power-voltage (Q-V) droop control scheme [3]. Similarly, the active power-voltage ($P_{\rm dc}$–$V_{\rm dc}$) droop control scheme is commonly used in dc MGs [4]. The HMG control method presented in [1], which in this article is referred to as the conventional control scheme of HMG, adopts the P-f/Q-V and $P_{\rm dc}$–$V_{\rm dc}$ droop control methods for the ac and dc subgrids, respectively. The operation of dc and ac MGs is coordinated by controlling the power flow through IC such that both ac and dc DERs respond to demand changes in each of the subgrids. To that end, the reference power of the IC is adjusted such that the per-unit (pu) frequency deviation in the ac MG becomes equal to the pu voltage deviation in dc MG. IC tracks the reference power by adopting the current control mode scheme. This technique coordinates the P-f droop controllers of ac DERs with the $P_{\rm dc}$–$V_{\rm dc}$ droop controllers of dc DERs such that the pu active power outputs of ac and dc DERs become equal. Consequently, each of ac and dc DERs participates in supplying the total HMG demand in accordance with its capacity. This condition, which is referred to as global power sharing, enhances the utilization factor of the DERs in spite of load variations in the ac and dc subgrids [5].

The conventional HMG control method is simple to implement and easy to design. However, the slow dynamics [6] and high-frequency fluctuations [7] degrade the performance of this method in practice. To enhance the dynamics of the HMG, a modified version of conventional droop method with feedforward current control loop for IC is presented in [8]. In [9], the IC is controlled to behave as a converter-based transformer (transfverter) which regulates the power transfer between the subgrids in accordance with different operation modes. In [10], a droop control scheme based on $f - V_{\rm dc}^2$ droop characteristics is proposed for IC. This method takes into account the intrinsic dynamics of the dc bus capacitor and the practical limitations of the frequency and dc bus voltage. In [11], a

Manuscript received August 27, 2020; revised November 27, 2020; accepted January 2, 2021. Date of publication January 8, 2021; date of current version May 5, 2021. Recommended for publication by Associate Editor G. Oriti. *(Corresponding author: Mohammad S. Golsorkhi.)*

Mohammad S. Golsorkhi is with the Department of Electrical and Computer Engineering, Isfahan University of Technology, Isfahan 8415683111, Iran (e-mail: golsorkhi@iut.ac.ir).

Mehdi Savaghebi is with the Electrical Engineering Section, Department of Mechanical and Electrical Engineering, University of Southern Denmark, Odense 5230, Denmark (e-mail: mesa@sdu.dk).

Color versions of one or more figures in this article are available at https://doi.org/10.1109/TPEL.2021.3049813.

Digital Object Identifier 10.1109/TPEL.2021.3049813

modified current controller is proposed for the IC to enhance the dynamic response and robustness with respect to disturbances. A comprehensive inertial control strategy for HMGs is proposed in [12]. This scheme exploits the kinetic inertia of wind turbines and the capacity of hybrid energy storage systems to improve the stability of the system. However, this method neglects the impact of network impedance and has a complex control structure. In [13], a local control method has been proposed for IC, in which the reference active power of IC is calculated as a weighted sum of the measured IC active power, the frequency deviation in ac MG, and the voltage deviation in dc MG. The controller parameters are adjusted based eigenvalue analysis to enhance the stability and power sharing accuracy.

Since the methods of [1], [8]–[13] operate the IC in current control mode, they provide limited voltage and frequency support for the ac subgrid during transients. Furthermore, the use of phase-locked loop (PLL) for sensing the frequency adds an unwanted delay in the IC control loop of these methods. To circumvent these issues, the voltage control mode has been proposed for IC [14]. Furthermore, to improve the capability of IC in supporting the ac subgrid frequency during transients, synchroconverter-based control scheme is proposed for IC [15]. In this method, the reference voltage of IC ac bus is obtained by the outer control loop such that IC mimics a synchronous machine, which changes its power in accordance with the global power sharing requirement. In [16], the synchroconverter concept is further developed to enable exploiting the inertia of synchronous generators in the ac subgrid as a short-term storage for enhancing the transient performance. In [17], a combination of virtual inertia in ac subgrid and virtual capacitance in dc subgrid are employed to further exploit the capacity of the sources for enhancing the stability of the system. To improve the power sharing accuracy in HMGs, an optimal power flow based power sharing strategy is proposed in [18]. In this method, the parameters of the DER and IC controllers are adjusted based on optimal power flow calculations. However, the implementation of this method requires a detailed model of the entire HMG, which may be difficult to obtain due to parameter uncertainties or modifications applied in the network, DERs, or loads over the utilization period of the HMG.

In this article, a novel decentralized control strategy is proposed. In this scheme, the V-I droop control scheme of [19] is adopted for ac subgrid, where the ac DERs and IC are synchronized to a global synchronous rotating reference frame by using GPS timing technology. To enable proportional load sharing among the ac DERs, the direct (d) and quadrature (q) components of their output voltages are determined based on the d and q components of the current according to a V-I droop characteristics. A similar V-I droop characteristic is used for dc DERs. The V-I droop method has some key advantages with respect to the conventional droop schemes (P-f and Q-V droop for ac and P-$V_{\rm dc}$ droop for dc sources), which are adopted in [1]–[18]. First, the direct incorporation of the output current (rather than power) in the droop characteristics reduces the delay associated with the power calculation and averaging. So the V-I droop method offers a faster dynamic response. Second, this method adopts a piecewise linear droop function with increasing slope to enhance the sharing accuracy at higher loading condition, where the sources are susceptible to overcurrent stresses. Third, thanks to the adaptation of GPS timing technology, the frequency deviations in the ac MG are eliminated. A new droop control law is proposed for the IC, in which the reference of the d-component of the IC ac bus voltage is calculated as a function of the IC dc bus voltage. This IC control strategy facilitates aligning the droop characteristics of ac and dc sources such that their pu output powers become equal. Hence, global power sharing among ac and dc sources is realized.

The contributions of the article are as follows.

1) Unlike [1], [8]–[13], [18], the proposed IC control method does require the measurement of IC ac bus frequency. So the PLL is eliminated from the power control loop and the delay associated with frequency measurement is removed. In addition, thanks to the utilization of V-I droop control strategy for ac and dc sources, the voltages of ac and dc subgrids respond quickly to the load variations. These features enable the IC to provide a faster dynamic response to load variations in each subgrid.
2) Compare with the methods of [14]–[17], the proposed scheme is simpler in structure and thanks to its piecewise linear droop characteristic, offers better sharing accuracy at high loading conditions.
3) In order to prove the stability of the proposed method despite the nonlinearity of the droop characteristics and the plant dynamics, Lyapunov stability analysis is presented. The analysis results are then used to devise a guideline for controller design.

The rest of the article is organized as follows. The proposed control scheme is addressed in Section II. Section III details the Lyapunov stability analysis of the proposed method. Simulation and experimental results are presented in Sections IV and V, respectively. Finally, Section VI concludes the article.

II. Proposed Control Scheme

Fig. 1 depicts the schematics of an HMG with associated control loops. The HMG is comprised of a dc and an ac subgrid. Each subgrid includes a number of DERs and loads interconnected through a distribution network. A bidirectional dc/ac converter (denoted as IC) connects the subgrids. The proposed control schemes for ac and dc DERs as well as IC are detailed in the following text.

A. V-I Droop Control Method of AC DERs

In the ac MG, V-I droop control method of [19] is adopted to enable proportional sharing of the load active and reactive power among DERs. In this method, GPS timing technology is employed to synchronize the ac DERs to a common rotating reference frame. This way, the frequency of the ac MG can be fixed at the rated value. The d and q axes components of the DER reference voltages are obtained as follows [20]:

$$\begin{bmatrix} v_{d,i}^{*} \\ v_{q,i}^{*} \end{bmatrix} = \begin{bmatrix} E_{\rm ac} \\ 0 \end{bmatrix} - \begin{bmatrix} m_d & 0 \\ 0 & m_q \end{bmatrix} \begin{bmatrix} g\left(i_{d,i} \big/ I_{d,i}^{\rm rated}\right) \\ h\left(i_{q,i} \big/ I_{q,i}^{\rm rated}\right) \end{bmatrix} \quad (1)$$

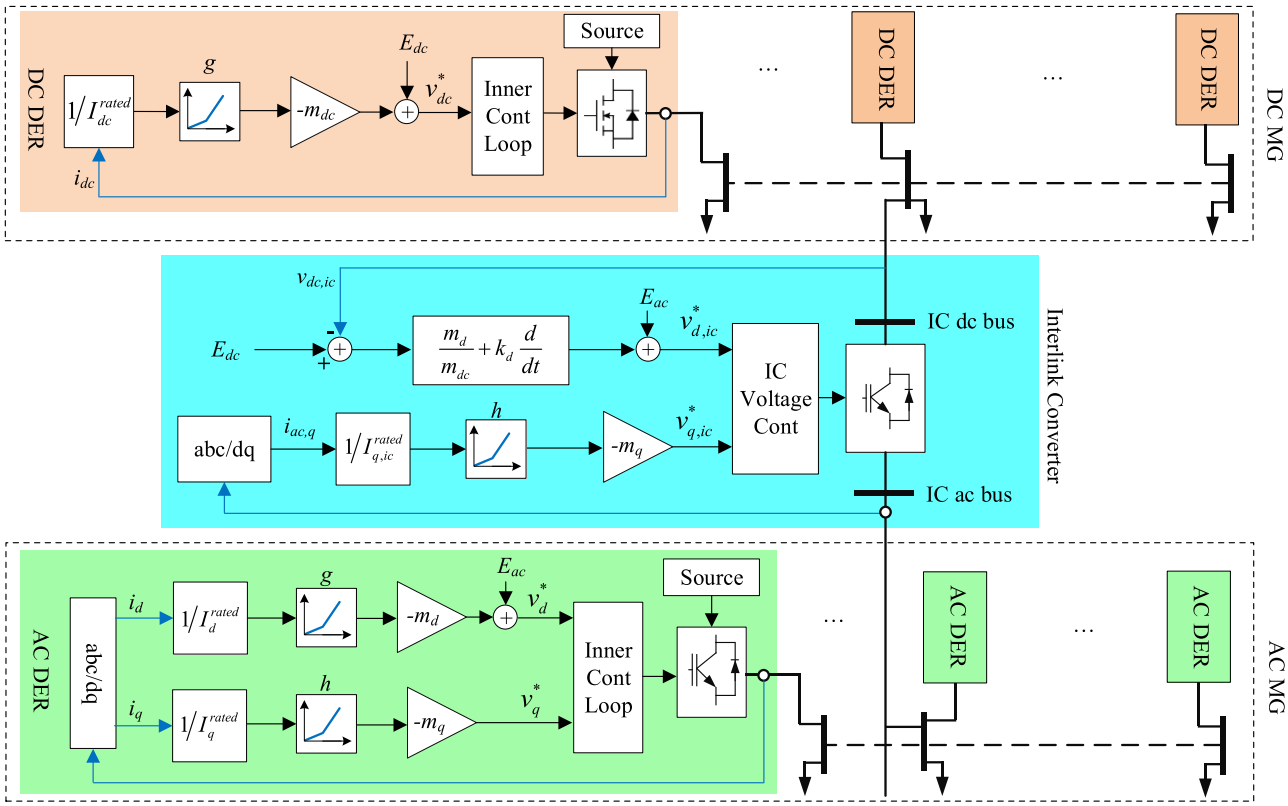

Fig. 1. Schematic diagram of proposed control scheme.

where $v^*_{d,i}$, $v^*_{q,i}$,$i_{d,i}$, $i_{q,i}$, $I^{\text{rated}}_{d,i}$, and $I^{\text{rated}}_{q,i}$ are the d and q components of, respectively, the reference voltage, output current, and the rated current of the ith ac DER unit. The parameters m_d and m_q are the d and q axis droop coefficients and E_{ac} is the amplitude of the no-load ac voltage. The functions g and h are one-to-one piece-wise linear droop functions, with $g(0) = h(0) = 0$ and $g(1) = h(1) = 1$.

According to IEEE standard 1159, the maximum voltage deviation in distribution networks is 10% [21]. Here, E_{ac} is selected as 1.05 of nominal voltage and m_d is selected as 0.1 pu to have the DER output voltage between 0.95 and 1.05 pu. The selection of a tighter range for the voltage deviation helps improve the voltage regulation and enables maintaining the voltage at the load buses within the acceptable range despite voltage drop across the distribution lines. The droop coefficient m_q is selected such that the internal dynamics of the ac DERs is stable; typically, $m_q I^{\text{rated}}_{q2}$ is around 10% to 20% of E_{ac} [19].

If the line voltage drops are neglected, the output voltages of the ac DERs ($v_{d,i}$, $v_{q,i}$) can be assumed to be equal. So, (1) implies the pu output currents of the ac DERs are also equal:

$$\frac{i_{d,1}}{I^{\text{rated}}_{d,1}} = \frac{i_{d,2}}{I^{\text{rated}}_{d,2}} = \cdots = \frac{i_{d,Nac}}{I^{\text{rated}}_{d,Nac}} \tag{2}$$

$$\frac{i_{q,1}}{I^{\text{rated}}_{q,1}} = \frac{i_{q,2}}{I^{\text{rated}}_{q,2}} = \cdots = \frac{i_{q,Nac}}{I^{\text{rated}}_{q,Nac}}. \tag{3}$$

where N_{ac} is the numbers of ac DERs. Since $v_d \approx 1$ pu and $v_q \approx 0$, the pu active and reactive power outputs of each DER are approximately equal to the pu values of i_d and i_q. So, (2) and (3) imply that the active and reactive power of the load is shared among the DERs in proportion to their capacities.

In the presence of impedances, the line voltages and hence the voltage differences at DER outputs increases with the increase of load. To enhance the sharing accuracy at high loading conditions, where the DERs are susceptible to overload, the slopes of the functions g and h are increased with the increase of load (please see [19] for more details). Due to its fast dynamic response and improved sharing accuracy at high loading, the V-I droop control scheme prevents overcurrent stresses during steady state and transients.

Although the proposed control scheme depends on GPS signal for synchronization of DERs, short-term GPS interruptions are tolerable by the proposed scheme. In the case of a long-term GPS failure, the modified V-I droop control scheme of [22] can be adopted to ensure stable operation.

B. V-I Droop Control Method of DC DERs

In case of dc DERs, the reference voltages are determined based on the following droop characteristics:

$$v^*_{\text{dc},i} = E_{\text{dc}} - m_{\text{dc}} g\left(\frac{i_{\text{dc},i}}{I^{\text{rated}}_{\text{dc},i}}\right) \tag{4}$$

where $v^*_{\text{dc},i}$, $i_{\text{dc},i}$, and $I^{\text{rated}}_{\text{dc},i}$ are, respectively, the reference voltage, output current, and the rated current of the ith dc DER unit. Furthermore, E_{dc} is the no-load dc output voltage and m_{dc}

is the dc droop coefficient. Similar to the case of ac DERs, the droop coefficient $m_{\rm dc}$ is selected such that the maximum voltage deviation does not exceed 10%.

C. IC Control Strategy

As mentioned before, the pu active power of ac DERs is approximately equal to $i_{d,\rm pu}$. Similarly, the pu power of dc DERs is approximately equal to $i_{\rm dc,pu}$. So the global power sharing among the ac and dc DERs can be interpreted as

$$\frac{i_{d,1}}{I_{d,1}^{\rm rated}} = \ldots = \frac{i_{d,N\rm ac}}{I_{d,N\rm ac}^{\rm rated}} = \frac{i_{\rm dc,1}}{I_{\rm dc,1}^{\rm rated}} = \ldots = \frac{i_{\rm dc,N dc}}{I_{\rm dc,N dc}^{\rm rated}} \tag{5}$$

where $N_{\rm dc}$ is the number of dc DERs. Comparing (1) and (4), it can be found that a sufficient condition for realizing (5) is

$$\forall i \in \{1,\ldots,N_{\rm ac}\}, \forall j \in \{1,\ldots,N_{\rm dc}\}:$$
$$\frac{v_{d,i} - E_{\rm ac}}{m_d} = \frac{v_{{\rm dc},j} - E_{\rm dc}}{m_{\rm dc}}. \tag{6}$$

If the line impedances are neglected, the IC ac (dc) bus voltage is equal to the ac (dc) DERs output voltages. So (6) can be simplified to

$$\frac{v_{d,\rm ic} - E_{\rm ac}}{m_d} = \frac{v_{\rm dc,ic} - E_{\rm dc}}{m_{\rm dc}} \tag{7}$$

where $v_{d,\rm ic}$ and $v_{\rm dc,ic}$ are the d-component of the ac bus voltage and the dc bus voltage of IC, respectively.

To realize (7), the d-component of the IC ac bus reference voltage ($v_{d,\rm ic}^*$) is calculated according to the following equation:

$$v_{d,\rm ic}^* = E_{\rm ac} + \frac{m_d}{m_{\rm dc}}\left(v_{\rm dc,ic} - E_{\rm dc}\right). \tag{8}$$

At steady-state condition, (8) enforces global power sharing by equalizing the relative deviations of v_d and $v_{\rm dc}$. However, the dc subgrid voltage tends to change with a slower rate than that of d-component of ac subgrid voltage due to the relatively large size of the dc capacitors at the IC dc bus and dc DERs outputs. This might result in slowing down the IC controller. To avoid this issue, a derivative term is added to the right-hand side of (8) to obtain the following IC droop control law:

$$v_{d,\rm ic}^* = E_{\rm ac} + \left(\frac{m_d}{m_{\rm dc}} + k_d\frac{d}{dt}\right)\left(v_{\rm dc,ic} - E_{\rm dc}\right) \tag{9}$$

in which k_d is the derivative gain.

To enable IC cooperate with ac DERs in supplying the reactive power of ac loads, the q-axis component of the IC ac bus voltage is controlled based on the following v_q–i_q droop control law:

$$v_{q,\rm ic}^* = -m_q h\left(\frac{i_{q,\rm ic}}{I_{q,\rm ic}^{\rm rated}}\right). \tag{10}$$

III. Stability Analysis

A. Mathematical Model of the System

In order to study the stability of the proposed control scheme, a reduced order model of HMG is used, as shown in Fig. 2. Here, the dynamics of the DERs' internal control loops are neglected as they are much faster than the power control dynamics [23].

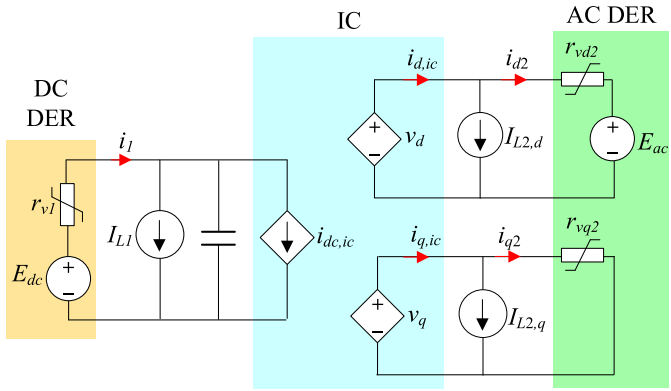

Fig. 2. Reduced order model of HMG.

According to (1) and (4), DERs can be modeled as nonideal voltage sources, which can be expressed as the combination of ideal voltage sources and the following nonlinear virtual resistances:

$$r_{v\rm dc} = \frac{m_{\rm dc}}{i_{\rm dc}} g\left(\frac{i_{\rm dc}}{I_{\rm dc}^{\rm rated}}\right) \tag{11}$$

$$r_{vd} = \frac{m_d}{i_d} g\left(\frac{i_d}{I_d^{\rm rated}}\right) \tag{12}$$

$$r_{vq} = \frac{m_q}{i_q} h\left(\frac{i_q}{I_q^{\rm rated}}\right). \tag{13}$$

For the sake of brevity, the combination of dc DERs is expressed as an aggregated dc DER model, which is comprised of a voltage source ($E_{\rm dc}$) and a nonlinear virtual resistance, r_{v1}. The ac DERs are modeled similarly. Furthermore, the line impedances are neglected because of their relatively small values compared with the virtual impedance of the DERs.

In the following text, the dc and ac DERs are denoted as DER1 and 2, respectively. Using KCL and KVL on the dc bus of Fig. 2, the capacitor current and voltage can be expressed as

$$C\frac{dv_{\rm dc}}{dt} = i_1 - i_{\rm dc,ic} - I_{L1} \tag{14}$$

$$v_{\rm dc} = E_{\rm dc} - r_{v1}\left(i_1\right) i_1. \tag{15}$$

Substituting (11) into (15) and solving for i_1, we have

$$i_1 = I_1^{\rm rated} g^{-1}\left(\frac{E_{\rm dc} - v_{\rm dc}}{m_{\rm dc}}\right). \tag{16}$$

The KVL equations on the ac buses are expressed as

$$v_d = E_{\rm ac} - r_{vd2} i_{d2} \tag{17}$$

$$v_q = -r_{vq2} i_{q2}. \tag{18}$$

Substituting (12) and (13) into (17) and (18) and solving for the DER2 current, we have

$$i_{d2} = I_{d2}^{\rm rated} g^{-1}\left(\frac{E_{\rm ac} - v_d}{m_d}\right) \tag{19}$$

$$i_{q2} = I_{q2}^{\rm rated} h^{-1}\left(-v_q/m_q\right). \tag{20}$$

By applying KCL on the ac buses and using (19), (20), the IC ac bus currents are obtained as

$$i_{d,\mathrm{ic}} = I_{L2,d} - I_{d2}^{\mathrm{rated}} g^{-1}\left(\frac{E_{\mathrm{ac}} - v_d}{m_d}\right) \tag{21}$$

$$i_{q,\mathrm{ic}} = I_{L2,q} - I_{q2}^{\mathrm{rated}} h^{-1}\left(-v_q/m_q\right). \tag{22}$$

Neglecting the power losses of the IC, it can be inferred that the power absorbed (or injected) from the IC dc bus is equal to the active power injected (or absorbed) into the IC ac bus. Mathematically,

$$v_d i_{d,\mathrm{ic}} + v_q i_{q,\mathrm{ic}} = v_{\mathrm{dc}} i_{\mathrm{dc,ic}}. \tag{23}$$

So, the current $i_{\mathrm{dc,ic}}$ can be expressed as

$$i_{\mathrm{dc,ic}} = \frac{v_d i_{d,\mathrm{ic}} + v_q i_{q,\mathrm{ic}}}{v_{\mathrm{dc}}}. \tag{24}$$

Combining (14), (16), (21), (22), and (24), we have

$$\begin{aligned} C\frac{dv_{\mathrm{dc}}}{dt} = & -I_{L1} + I_1^{\mathrm{rated}} g^{-1}\left(\frac{E_{\mathrm{dc}} - v_{\mathrm{dc}}}{m_{\mathrm{dc}}}\right) \\ & - \left(I_{L2,d} - I_{d2}^{\mathrm{rated}} g^{-1}\left(\frac{E_{\mathrm{ac}} - v_d}{m_d}\right)\right)\frac{v_d}{v_{\mathrm{dc}}} \\ & - \left(I_{L2,q} - I_{q2}^{\mathrm{rated}} h^{-1}\left(\frac{-v_q}{m_q}\right)\right)\frac{v_q}{v_{\mathrm{dc}}}. \end{aligned} \tag{25}$$

Equation (25) represents the dynamics of the HMG in terms of the state variables v_{dc}, v_d, and v_q. From (1) and (4), the equilibrium value of the states can be expressed as

$$V_{\mathrm{dc}} = E_{\mathrm{dc}} - m_{\mathrm{dc}} g\left(I_1/I_1^{\mathrm{rated}}\right) \tag{26}$$

$$V_d = E_{\mathrm{ac}} - m_d g\left(I_{d2}/I_{d2}^{\mathrm{rated}}\right) \tag{27}$$

$$V_q = -m_q h\left(I_{q2}/I_{q2}^{\mathrm{rated}}\right). \tag{28}$$

To use Lyapunov stability theorem, a change of variables is used to have the equilibrium of the system at the origin. In particular, the new states x, y, and z are defined as $x = v_{\mathrm{dc}} - V_{\mathrm{dc}}$, $y = v_d - V_d$, and $z = v_q - V_q$. By changing the state variables to x, y, and z and using (26)–(28), (25) can be expressed as

$$\begin{aligned} C\frac{dx}{dt} = & -I_{L1} + I_1^{\mathrm{rated}} g^{-1}\left(g\left(\frac{I_1}{I_1^{\mathrm{rated}}}\right) - \frac{x}{m_{\mathrm{dc}}}\right) \\ & - \left(I_{L2,d} - I_{d2}^{\mathrm{rated}} g^{-1}\left(g\left(\frac{I_{d2}}{I_{d2}^{\mathrm{rated}}}\right) - \frac{y}{m_d}\right)\right)\frac{y + V_d}{x + V_{\mathrm{dc}}} \\ & - \left(I_{L2,q} - I_{q2}^{\mathrm{rated}} h^{-1}\left(h\left(\frac{I_{q2}}{I_{q2}^{\mathrm{rated}}}\right) - \frac{z}{m_q}\right)\right)\frac{z + V_q}{x + V_{\mathrm{dc}}}. \end{aligned} \tag{29}$$

At steady-state conditions, where x, y, z and their derivatives converge to zero, (29) implies that $V_{\mathrm{dc}}(I_1 - I_{L1}) = V_d(I_{d2} - I_{L2,d}) + V_q(I_{q2} - I_{L2,q})$. This result states the power balance in the HMG.

If functions $c_1(x)$, $c_2(y)$, and $c_3(z)$ are defined as

$$\begin{aligned} c_1(x) &= I_1 - I_1^{\mathrm{rated}} g^{-1}\left(g\left(\frac{I_1}{I_1^{\mathrm{rated}}}\right) - \frac{x}{m_{\mathrm{dc}}}\right) \\ c_2(y) &= I_{d2} - I_{d2}^{\mathrm{rated}} g^{-1}\left(g\left(\frac{I_{d2}}{I_{d2}^{\mathrm{rated}}}\right) - \frac{y}{m_d}\right) \\ c_3(z) &= I_{q2} - I_{q2}^{\mathrm{rated}} h^{-1}\left(h\left(\frac{I_{q2}}{I_{q2}^{\mathrm{rated}}}\right) - \frac{z}{m_q}\right). \end{aligned} \tag{30}$$

Then, (29) can be written as follows:

$$\begin{aligned} C\frac{dx}{dt} = & -\left(\frac{c_1(x)}{x} - \frac{I_{\mathrm{dc,ic}}}{x + V_{\mathrm{dc}}}\right)x - \left(\frac{c_2(y)}{y}\frac{y + V_d}{x + V_{\mathrm{dc}}} + \frac{I_{d,\mathrm{ic}}}{x + V_{\mathrm{dc}}}\right)y \\ & - \left(\frac{c_3(z)}{z}\frac{z + V_q}{x + V_{\mathrm{dc}}} + \frac{I_{q,\mathrm{ic}}}{x + V_{\mathrm{dc}}}\right)z. \end{aligned} \tag{31}$$

The reference value of the d-component of the IC ac voltage is determined based on the IC droop function (9). As shown in Fig. 1, the reference voltage is fed to the IC voltage control loop. The dynamics of the IC voltage controller can be approximated by the following first-order equations [24]:

$$\tau_d \frac{dv_d}{dt} + v_d = v_d^* \tag{32}$$

$$\tau_q \frac{dv_q}{dt} + v_q = v_q^* \tag{33}$$

where τ_d and τ_q are the time constants of the d and q axis of voltage control loops. Substituting (9) into (32) gives

$$\tau_d \frac{dv_d}{dt} + v_d = E_{\mathrm{ac}} + \frac{m_d}{m_{\mathrm{dc}}}\left(v_{\mathrm{dc}} - E_{\mathrm{dc}}\right) + k_d \frac{d}{dt} v_{\mathrm{dc}}. \tag{34}$$

By change of variables, (34) can be expressed in terms of x, y, and z, as follows:

$$\begin{aligned} & \tau_d \frac{dy}{dt} + y + E_{\mathrm{ac}} - m_d g\left(\frac{I_{d2}}{I_{d2}^{\mathrm{rated}}}\right) \\ & = E_{\mathrm{ac}} + \frac{m_d}{m_{\mathrm{dc}}}\left(x + E_{\mathrm{dc}} - m_{\mathrm{dc}} g\left(\frac{I_1}{I_1^{\mathrm{rated}}}\right) - E_{\mathrm{dc}}\right) \\ & + k_d \frac{d}{dt} x. \end{aligned} \tag{35}$$

Since the global power sharing condition of (5) is satisfied at steady state ($I_{d2}/I_{d2}^{\mathrm{rated}} = I_1/I_1^{\mathrm{rated}}$), (35) can be simplified to

$$\tau_d \frac{dy}{dt} = -y + \frac{m_d}{m_{\mathrm{dc}}} x + k_d \frac{dx}{dt}. \tag{36}$$

Substituting (10) into (33) gives

$$\tau_q \frac{dv_q}{dt} + v_q = -m_q h\left(\frac{i_{q,\mathrm{ic}}}{I_{q,\mathrm{ic}}^{\mathrm{rated}}}\right). \tag{37}$$

By substituting $i_{q,\mathrm{ic}}$ with the right-hand side of (22), (37) can be expressed as

$$\tau_q \frac{dz}{dt} = -z - c_4(z) \tag{38}$$

in which

$$c_4(z) = m_q\left(h\left(\frac{c_3(z)+I_{q,ic}}{I_{q,ic}^{\text{rated}}}\right)-h\left(\frac{I_{q2}}{I_{q2}^{\text{rated}}}\right)\right). \quad (39)$$

B. Lyapunov Stability Analysis

Equations (31), (36), and (38) express the system dynamics in terms of nonlinear differential equations. In this subsection, the stability of the system is studied by using Lyapunov stability theorem [25]. A positive definite Lyapunov function is defined in terms of the state variables *x, y,* and *z*. By selecting the control parameters such that the time derivative of Lyapunov function is negative definite, asymptotic stability is guaranteed. In the following text, first the upper bounds of expressions c_1–c_4 are derived (see Theorems 1 and 2). Then, these upper bounds are used in Theorem 3 to prove the system is asymptotically stable.

Theorem 1: If the functions *g* and *h* are strictly increasing piecewise linear with maximum slopes a_g and a_h, then for any nonzero *x*, *y*, *z*, the expressions $c_1(x)/x$, $c_2(y)/y$,and $c_3(z)/z$ have positive lower bounds, as follows:

$$\frac{c_1(x)}{x} \geq \frac{I_1^{\text{rated}}}{a_g m_{\text{dc}}} \quad (40)$$

$$\frac{c_2(y)}{y} \geq \frac{I_{d2}^{\text{rated}}}{a_g m_d} \quad (41)$$

$$\frac{c_3(z)}{z} \geq \frac{I_{q2}^{\text{rated}}}{a_h m_q}. \quad (42)$$

Proof: Since the function *g* is strictly increasing with maximum slope a_g, the inverse of *g* is also strictly increasing with minimum slope $1/a_g$. Therefore, the slope of the line connecting a pair of points on g^{-1} is greater than $1/a_g$. Mathematically,

$$\frac{g^{-1}(w+\Delta w)-g^{-1}(w)}{\Delta w} < \frac{1}{a_g}. \quad (43)$$

Substituting *w* with $g(I_1/I_1^{\text{rated}})$ and Δw with $-x/m_{\text{dc}}$, (43) can be written as

$$\frac{g^{-1}\left(g\left(I_1/I_1^{\text{rated}}\right)-x/m_{\text{dc}}\right)-I_1/I_1^{\text{rated}}}{-x/m_{\text{dc}}} < \frac{1}{a_g} \quad (44)$$

which implies (40). The inequalities (41) and (42) can be driven in a similar fashion.

Theorem 2: For any nonzero *z*, the expression $c_4(z)/z$ is positive definite.

Proof: According to (42), $c_3(z)$ has the same sign as z. Consequently, if *z* is positive, $(c_3(z)+I_{q,\text{ic}})/I_{q,\text{ic}}^{\text{rated}} > I_{q,\text{ic}}/I_{q,\text{ic}}^{\text{rated}}$. Since the *q* axis current is proportionally shared among the ac DERs and IC ($I_{q,\text{ic}}/I_{q,\text{ic}}^{\text{rated}} = I_{q2}/I_{q2}^{\text{rated}}$) and *h* is strictly increasing, the mentioned inequality implies that $c_4(z)$ is positive. Alternatively, in the case of a negative *z*, $(c_3(z)+I_{q,\text{ic}})/I_{q,\text{ic}}^{\text{rated}} < I_{q,\text{ic}}/I_{q,\text{ic}}^{\text{rated}}$ and $c_4(z)$ is negative. Therefore, $c_4(z)/z$ is positive definite for any nonzero *z*.

Theorem 3: The dynamic system expressed by (31), (36), (38) is asymptotically stable if the controller parameters are selected such that $b_2^2+b_1>0$ and $b_2-\sqrt{b_2^2+b_1} < k_d/\tau_d < b_2+\sqrt{b_2^2+b_1}$ where

$$\begin{aligned} b_1 = &\left(\frac{4I_1^{\text{rated}}}{a_g m_{\text{dc}}}-\frac{4I_{\text{dc,ic}}^{\text{rated}}}{\min\{v_{\text{dc}}\}}\right) \\ &-\left(\frac{\max\{v_q\}}{\min\{v_{\text{dc}}\}}\cdot\frac{I_{q2}^{\text{rated}}}{a_h m_q}+\frac{I_{q,\text{ic}}^{\text{rated}}}{\min\{v_{\text{dc}}\}}\right)^2 \\ &-\left(\frac{m_d}{m_{\text{dc}}}+\frac{I_{d,\text{ic}}^{\text{rated}}}{\min\{v_{\text{dc}}\}}-\frac{I_{d2}^{\text{rated}}}{a_g m_d}*\frac{\min\{v_d\}}{\max\{v_{\text{dc}}\}}\right)^2 \end{aligned} \quad (45)$$

$$b_2 = \frac{m_d}{m_{\text{dc}}}+\frac{I_{d2}^{\text{rated}}}{a_g m_d}*\frac{\min\{v_d\}}{\max\{v_{\text{dc}}\}}-\frac{I_{d,\text{ic}}^{\text{rated}}}{\min\{v_{\text{dc}}\}}. \quad (46)$$

Proof: Consider the positive definite Lyapunov function candidate:

$$V = \frac{1}{2}Cx^2+\frac{1}{2\tau_d}(\tau_d y-k_d x)^2+\frac{1}{2}\tau_q z^2. \quad (47)$$

The derivative of *V* is calculated as follows:

$$\frac{dV}{dt} = xC\frac{dx}{dt}+\frac{1}{\tau_d}(\tau_d y-k_d x)\left(\tau_d\frac{dy}{dt}-k_d\frac{dx}{dt}\right)+z\tau_q\frac{dz}{dt}. \quad (48)$$

Substituting the derivative terms in (48) with (31), (36), (38) gives

$$\begin{aligned} \frac{dV}{dt} = &-\left(\frac{c_1(x)}{x}-\frac{I_{\text{dc,ic}}}{x+V_{\text{dc}}}+\frac{k_d}{\tau_d}\frac{m_d}{m_{\text{dc}}}\right)x^2 \\ &-\left(\frac{c_2(y)}{y}\frac{y+V_d}{x+V_{\text{dc}}}+\frac{I_{d,ic}}{x+V_{\text{dc}}}-\left(\frac{m_d}{m_{\text{dc}}}+\frac{k_d}{\tau_d}\right)\right)xy-y^2 \\ &-\left(\frac{c_3(z)}{z}\frac{z+V_q}{x+V_{\text{dc}}}+\frac{I_{q,\text{ic}}}{x+V_{\text{dc}}}\right)xz-\left(1+\frac{c_4(z)}{z}\right)z^2. \end{aligned} \quad (49)$$

By using Theorems 1 and 2, an upper bound for $dV/dt$is obtained as

$$\begin{aligned} \frac{dV}{dt} \leq &-\left(\frac{I_1^{\text{rated}}}{a_g m_{\text{dc}}}-\frac{I_{\text{dc,ic}}}{x+V_{\text{dc}}}+\frac{k_d}{\tau_d}\frac{m_d}{m_{\text{dc}}}\right)x^2 \\ &+\left(\frac{m_d}{m_{\text{dc}}}+\frac{k_d}{\tau_d}-\frac{c_2(y)}{y}\frac{y+V_d}{x+V_{\text{dc}}}-\frac{I_{d,\text{ic}}}{x+V_{\text{dc}}}\right)xy-y^2 \\ &-\left(\frac{I_{q2}^{\text{rated}}}{a_h m_q}\frac{z+V_q}{x+V_{\text{dc}}}+\frac{I_{q,\text{ic}}}{x+V_{\text{dc}}}\right)xz-z^2. \end{aligned} \quad (50)$$

The right-hand side of (50) is of the form $-a_1x^2+2a_2xy-y^2-2a_3zx-z^2$ which can be rearranged as $-(y-a_2x)^2-(a_1-a_2^2)x^2-2a_3xz-z^2$. The quadratic expression $-(a_1-a_2^2)x^2-2a_3xz-z^2$ is negative if $D=a_3^2-a_1+a_2^2$ is negative, i.e.,

$$\begin{aligned} D = &\left(\frac{m_d}{m_{\text{dc}}}+\frac{k_d}{\tau_d}-\frac{I_{d,\text{ic}}}{x+V_{\text{dc}}}-\frac{c_2(y)}{y}\frac{y+V_d}{x+V_{\text{dc}}}\right)^2 \\ &+\left(\frac{I_{q2}^{\text{rated}}}{a_h m_q}\frac{z+V_q}{x+V_{\text{dc}}}+\frac{I_{q,\text{ic}}}{x+V_{\text{dc}}}\right)^2 \\ &-4\left(\frac{I_1^{\text{rated}}}{a_g m_{\text{dc}}}-\frac{I_{\text{dc,ic}}}{x+V_{\text{dc}}}+\frac{k_d}{\tau_d}\frac{m_d}{m_{\text{dc}}}\right)<0. \end{aligned} \quad (51)$$

Using Theorem 1, and replacing the variables with their limits, an upper bound for D is obtained as

$$D \leq \left(\frac{m_d}{m_{\rm dc}} + \frac{I_{d,ic}^{\rm rated}}{\min\{v_{\rm dc}\}} - \frac{I_{d2}^{\rm rated}}{a_g m_d} * \frac{\min\{v_d\}}{\max\{v_{\rm dc}\}} + \frac{k_d}{\tau_d} \right)^2 + \left(\frac{\max\{v_q\}}{\min\{v_{\rm dc}\}} * \frac{I_{q2}^{\rm rated}}{a_h m_q} + \frac{I_{q,ic}^{\rm rated}}{\min\{v_{\rm dc}\}} \right)^2 - 4 \left(\frac{I_1^{\rm rated}}{a_g m_{\rm dc}} - \frac{I_{\rm dc,ic}^{\rm rated}}{\min\{v_{\rm dc}\}} + \frac{m_d}{m_{\rm dc}} \frac{k_d}{\tau_d} \right). \quad (52)$$

The above expression can be represented in the form $-b_1 - 2b_2 k_d/\tau_d + (k_d/\tau_d)^2$, in which b_1 and b_2 are shown in (45). If the term $b_2^2 + b_1$ is positive, the roots of right-hand side of (52) with respect to k_d/τ_d will be $b_2 \pm \sqrt{b_2^2 + b_1}$. Selecting k_d/τ_d between these roots ensures that the right-hand side of (52) and hence D is negative, which implies that dV/dt is negative definite. So the system is asymptotically stable.

C. Guidelines for Controller Design

The key control parameters, which affect the system stability, are the IC's inner control loops, DERs droop parameters, and the derivative coefficient of IC droop controller. The inner control inner control loops comprise of cascaded proportional plus resonant controllers. The design of inner control loop parameters have been extensively studied and standard design guidelines based on linear analysis tools have been presented in the literature [24]. Commonly, the inner loops are designed such that the voltage controller time constant (τ_d) is smaller than one power cycle. The droop controller parameters m_d and $m_{\rm dc}$ are equal to the maximum voltage deviation in dc and ac subgrids, respectively. The parameter m_q and the maximum slope of the q axis droop function (a_h) can be selected in accordance with the eigenvalue analysis presented in [17]. In order to improve the dynamic response of IC with respect to load changes in the dc subgrid, a positive derivative gain (k_d) must be used. This way, the derivative term can have a positive contribution in the droop control law. A sufficient condition for meeting the stability criterion of Theorem 3 with some positive k_d is having positive b_1 and b_2. This condition can be used as a guideline for selection of the maximum slope of the droop functions (a_g).

For the MG studied in Section IV, the inner control loops are designed such that $\tau_d \simeq 0.01$ s. In order to limit the voltage deviations to 10%, m_d and $m_{\rm dc}$ are selected as 31 and 75 V, respectively. Based on the analysis presented in [17], m_q is selected as 31 V and a_h is selected as 2. To have positive values for b_1 and b_2, a_g is selected as 2. The parameters b_1 and b_2 are found as 0.2 and 0.55, respectively. So based on Theorem 3, the system is stable as long as $k_d \in (-0.0016,\ 0.012)$. Here, k_d is selected as 0.005.

IV. Simulation Results

The conventional control scheme of [1] and the proposed control strategy are tested on a HMG supplies by five DERs of different capacities. Fig. 3 shows the schematic diagram of the HMG. The dc subgrid is comprised of two dc DERs and two dc loads, whereas the ac subgrid includes three ac DERs and two ac loads. The two subgrids are linked through an IC. Tables I and II list the electrical and control parameters of the HMG. The dc subgrid has a rated voltage of 750 V and the nominal parameters of ac subgrid are 220 V (phase to ground) and 50 Hz. In accordance with the resistive nature of the distribution networks, the *R/X* ratio of the line impedances are selected at around 7 [26]. For each of the DERs and IC, the rating, filter components, and control parameters are detailed in the table.

To have a fair comparison between the proposed scheme and the conventional control method of [1], the same inner control

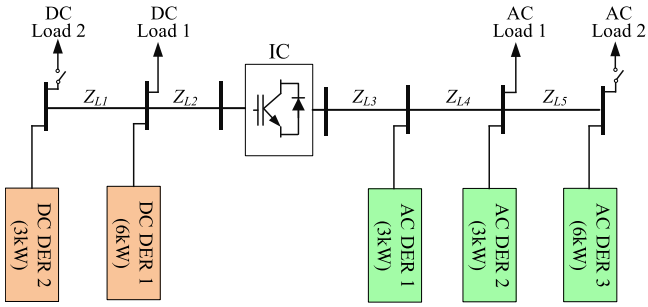

Fig. 3. Schematic diagram of simulated HMG.

TABLE I
Electrical Parameters of Simulated HMG

Description	Values
Rated Parameters	V_{ph}^{rated}= 220V , f^{rated}= 50Hz , V_{dc}=750 V
AC DER1, 2	P^{rated}= 3kW , $L_f = L_g$= 1.8mH , C_f= 5μF
AC DER 3, IC	P^{rated}= 6kW , $L_f = L_g$= 0.89mH , C_f= 10μF
DC DER 1	P^{rated}= 6kW L_f= 0.2 mH , C_f= 12.5μF
DC DER 2	P^{rated}= 3kW, L_f= 0.5 mH , C_f= 5μF
Line Impedances (Ω)	Z_{L1}= 0.4, Z_{L2}= 0.5, $Z_{L3} = Z_{L4}$= 0.05+*j*0.007, Z_{L5}= 0.03+*j*0.004
Load Impedances (Ω)	Z_{dc1}=300, Z_{dc2}=50 Z_{ac1}=30+*j*15, Z_{ac2}=19+*j*12

TABLE II
Control Parameters of Simulated HMG

Parameters of Inner Control Loops	
AC DER 1,2	k_{pi}= 8.5 , k_{ri}= 200, k_{pv}= 0.008 , k_{rv}=50
AC DER 3, IC	k_{pv}= 4.35 , k_{rv}= 99.5 , k_{pi}= 0.015 , k_{ri}=100
DC DER 1	k_{pi}= 4 , k_{ii}= 1000, k_{pv}= 0.01 , k_{iv}=100
DC DER 2	k_{pi}= 8 , k_{ii}= 2000, k_{pv}= 0.005 , k_{iv}=50
Parameters of Outer Control Loops (Conventional Method)	
DER Droop Controller	k_p= 0.08Hz/kW, k_q= 7.7V/kVAR k_p^{dc} =12.5V/kW
DER Virtual Impedance	Z_v=0.03+j0.06 pu
IC PLL	k_p= 180 , k_i= 3200 , k_d= 1
IC Power Controller	k_{pp}= 6000 , k_{ip}= 30000
Parameters of Outer Control Loops (Proposed Method)	
DER Droop Controller	m_d= 31V , m_q= 31V, m_{dc}= 75V
IC	k_d= 0.005

loops are used for both schemes. In addition, a virtual impedance (Z_v) is added in the control loops of the ac DERs of the conventional control method to ensure optimal performance in spite of resistive ac network impedance. The droop controller parameters of the conventional scheme are selected by considering the maximum permissible voltage and frequency deviations.

The simulation results for the conventional and proposed control scheme are shown in Figs. 4 and 5. Prior to $t = 0$ s, the dc load 1 and ac load 1 are connected to the network. From Figs. 4(a) and 5(a), it is seen that both methods satisfy the global power sharing condition with P_{ac3} and P_{dc2} being almost equal and double that of P_{ac1}, P_{ac2}, and P_{dc1}. A small active power sharing error is observable in both cases. However, thanks to adopting a nonlinear droop control law, the proposed control method favors reduced sharing error at higher loading conditions, when the DERs are susceptible to overload ($t > 1$ s). As shown in Figs. 4(b) and 5(b), the reactive power is shared proportionally among the ac DERs. However, comparing Fig. 4(b) and (c) reveals that the reactive power sharing among IC and ac DERs is poor in the conventional method. The reason is the lack of virtual impedance in the conventional IC control scheme. This problem is resolved in the proposed method.

At $t = 0$ s, a step load change is incurred in the ac MG by connecting the ac load 2. In the case of the conventional control method, the ac DERs first respond to this load change by increasing their output powers [see Fig. 4(a)]. The P-f droop controllers of ac DERs decrease the frequency, as shown in Fig. 4(f). This frequency drop is then sensed by the IC controller, which increases the IC active power [see Fig. 4(b)]. Subsequently, the dc DERs increase their output powers to maintain the power balance in dc subgrid. The relatively slow dynamics of the power control loop of the IC and the delay associated with the frequency measurement (PLL) delays the response of IC and hence the dc DERs. Consequently, as seen in Fig. 4(a), the step load change is first picked up by ac DERs and after several ac power cycles dc DERs take their share of the load. This sluggishness causes the ac DERs to undergo a transient power overshoot.

In contrast with the conventional droop method, the dynamic response of the proposed method is fast. When the ac load increases, the V-I droop controllers of ac DERs quickly decrease the d-component of the ac bus voltage and hence its rms value [see Fig. 5(e)]. Without any delay, this change is sensed by IC controller, which increases the IC active power, as shown in Fig. 5(c). The dc DERs respond to the IC action by increasing their output powers. Thanks to the fast dynamics of this process, the power overshoot of ac DERs is eliminated.

At $t = 1$ s, the dc load 2 is connected, resulting in a step load rise in the dc MG. From Fig. 4(a) and (c), it is observed that in the case of the conventional control method, for similar reasons stated in the above text, the step load change is first picked up by the dc DERs and the response of IC and ac DERs has a delay. So, the dc DERs experience a power overshoot. This overshoot is again avoided in the proposed control scheme, as shown in Fig. 5(a).

From Figs. 4(d) and (e) and 5(d) and (e), it is observed that in both conventional and proposed scheme, the voltages of dc and ac buses of the MG remain within the permissible range. This is a direct consequence of selecting the droop coefficients in accordance with the specified voltage limits. Comparing Figs. 4(f) and 5(f) reveals that unlike the conventional method, the proposed control method does not suffer from frequency deviations. The transient frequency fluctuations observed in Fig. 5(f) are caused by variations of d and q components of the DER voltages. Zero steady-state frequency deviation is a key feature of GPS-based control MG schemes and particularly the proposed method.

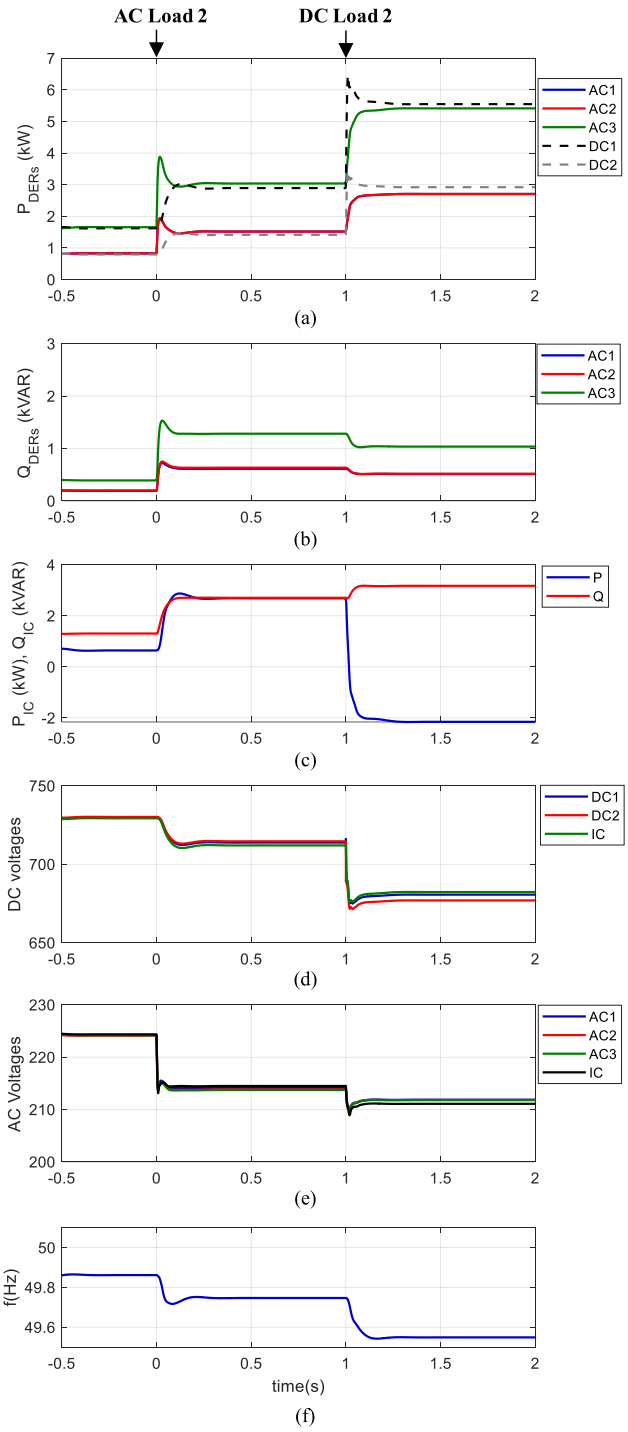

Fig. 4. Performance of conventional control method. (a) DERs active powers. (b) AC DERs reactive powers. (c) IC powers. (d), (e) DC/AC bus voltages. (f) Frequency.

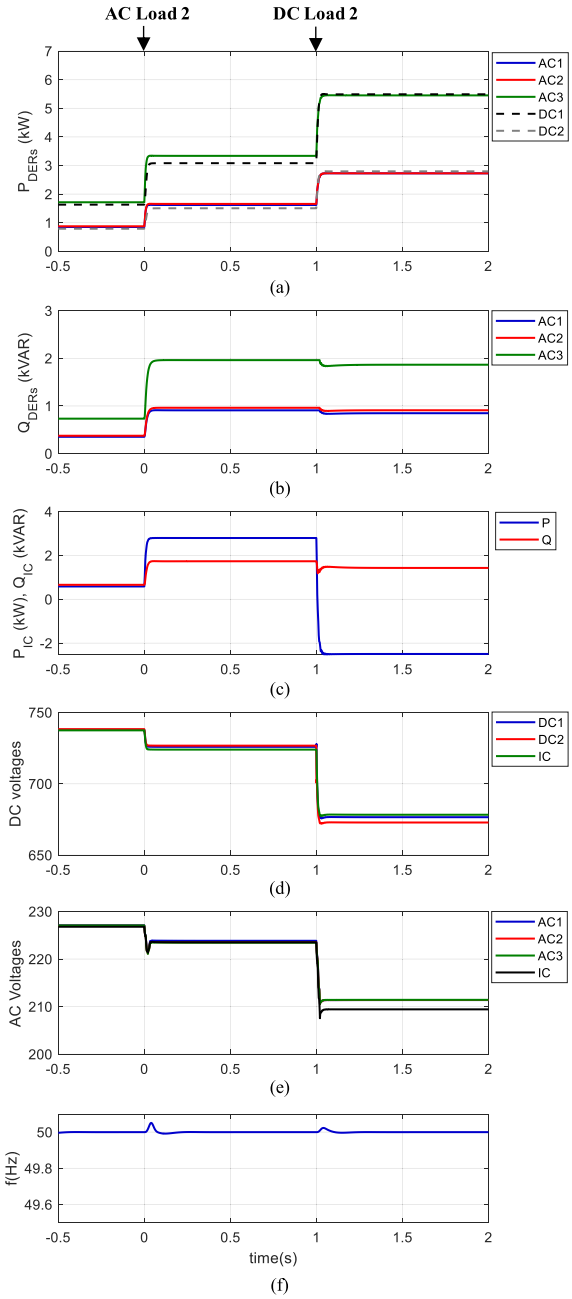

Fig. 5. Performance of proposed control method. (a) DERs active powers. (b) AC DERs reactive powers. (c) IC powers. (d), (e) DC/AC bus voltages. (f) Frequency.

V. Experimental Results

The proposed control strategy was tested in a laboratory-scale MG setup. As depicted in Fig. 6(a), the experimental setup is comprised of three main cabinets, one switch box and one control box. Inside the control box, there are three target PCs, each of which controls one of the cabinets. As shown in Fig. 6(b), five converters, including two three-phase inverters, two three-phase active front-end rectifiers, and one inverter with shorted outputs are placed inside each cabinet. Each converter is connected to an FPGA board, which communicates to target PCs via a fast optic fiber link. The target PCs, which serve as the main controller unit,

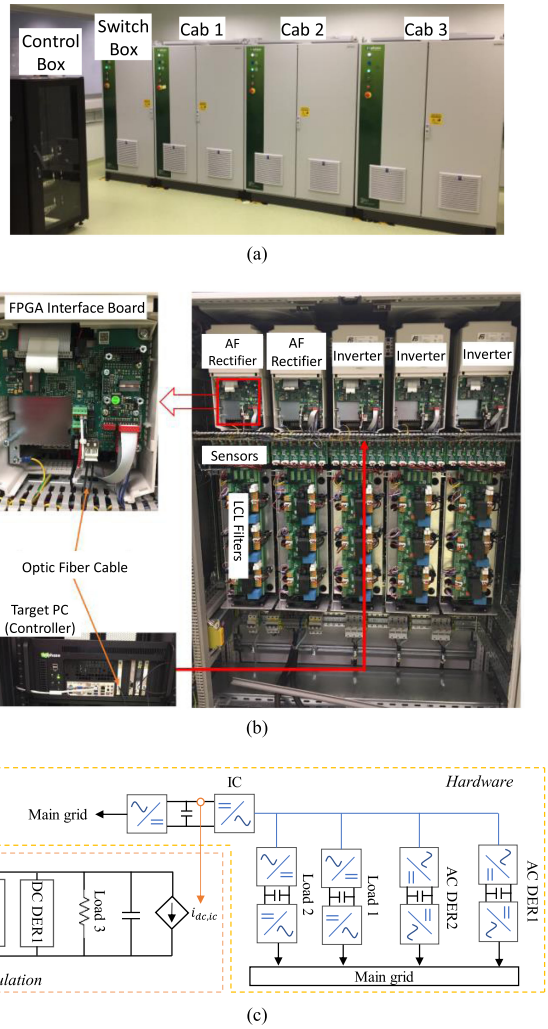

Fig. 6. Experimental setup. (a), (b) Photographs of hardware. (c) Schematic diagram.

receive feedback signals from the FPGA boards and calculate the reference of the PWM signals according to the proposed control scheme. Then, the FPGA boards generate PWM pulses, which are applied to the converters' switches.

Fig. 6(c) shows the schematic diagram of the HMG setup. As seen, two back to back converters are employed for implementation of the ac DERs, two are used as active controllable ac loads and one serves as IC. The ac DERs, IC, and dc DERs have a rated power of 6 kW and their specifications are identical with ac DER 3 and dc DER2 of the simulated MG (see Table I). The dc subgrid is emulated in the target PCs. The ac subgrid is interfaced with the dc subgrid by including the measured dc current of IC (hardware side) as a controllable dc current source in the dc subgrid.

The experimental results of the conventional and proposed method are shown in Figs. 7 and 8, respectively. Initially, the ac load consumes 7 kW (at power factor PF = 0.85) and the dc load is 3 kW. Since the dc load is lighter than the ac load, IC transfers around 2 kW from dc to ac subgrid [see Figs. 7(b) and 8(b)] to enable dc DERs contribute to the ac load. Therefore,

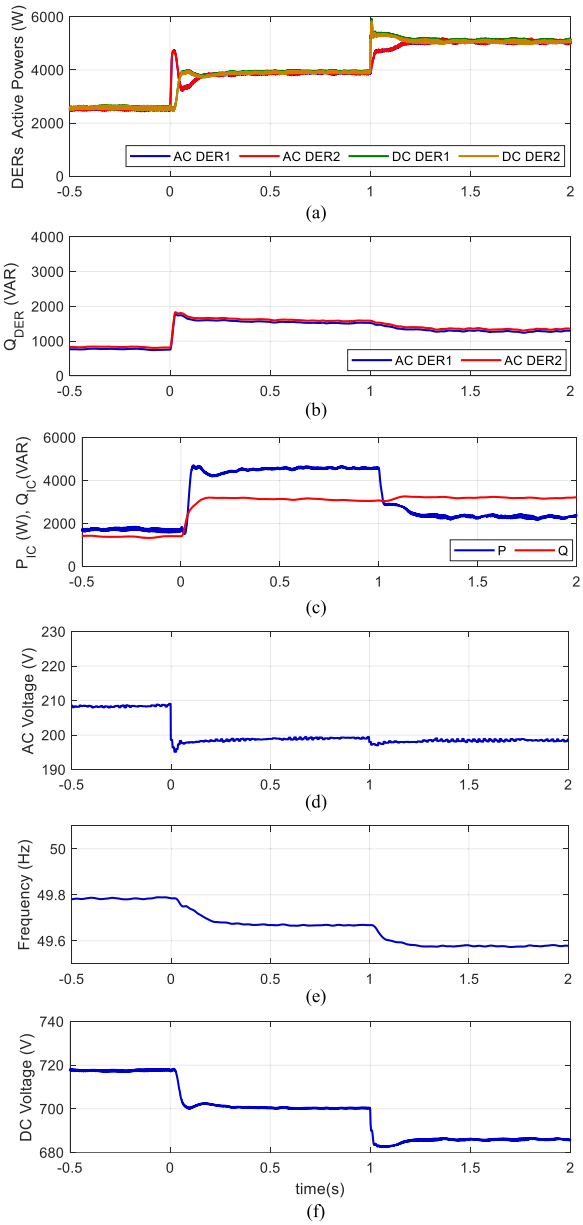

Fig. 7. Experimental results of conventional control method. (a) DERs active powers. (b) AC DERs reactive powers. (c) IC active/reactive power. (d) AC voltage. (e) Frequency. (f) DC voltage.

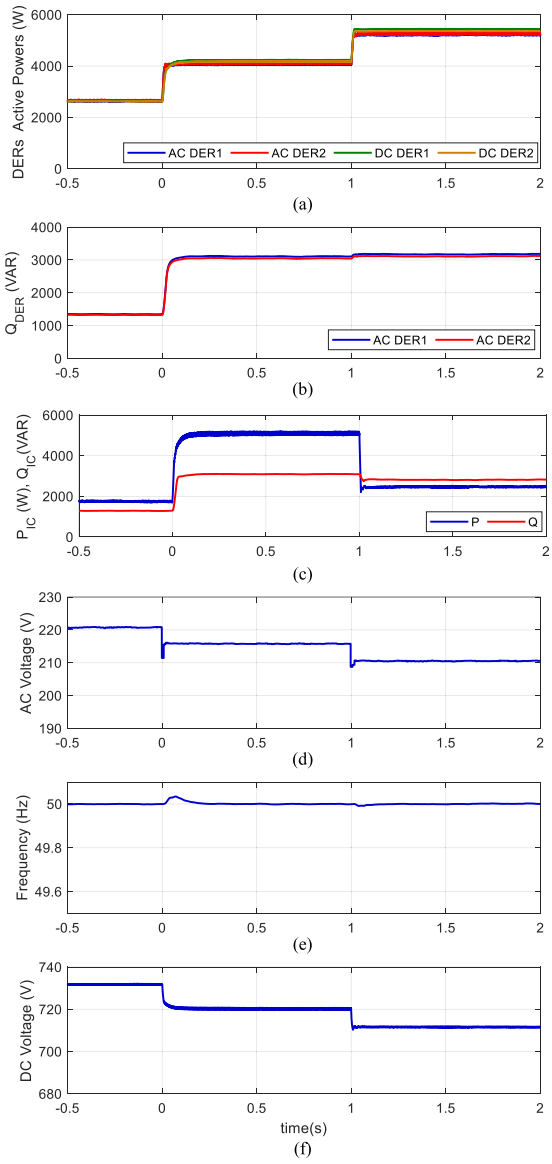

Fig. 8. Experimental results of proposed control method. (a) DERs active powers. (b) AC DERs reactive powers. (c) IC active/reactive power. (d) AC voltage. (e) Frequency. (f) DC voltage.

the output powers of ac and dc DERs become equal. In other words, global power sharing is satisfied. At $t = 0$ s, the ac load is increased from 7 to 14 kW (PF $= 0.85$). To maintain global power sharing, the IC active power increases to around 5 kW, hence allowing the dc DERs to contribute to this load rise. At $t = 1$ s, the dc load is changed from 3 to 8 kW. This time, the IC active power decreases to around 2.2 kW. Consequently, the active power output of ac and dc DERs merge at the same value.

Comparison of Figs. 4 and 5 with Figs. 7 and 8 reveals that the experimental results verify the simulations. Here, similar to the simulation results, the proposed method favors a smooth and overshoot-free transient response. Furthermore, zero frequency deviation is achieved in the proposed scheme.

VI. Conclusion

HMGs are an attractive solution for the integration of dc and ac DERs and loads in smart distribution systems. HMGs are comprised of dc and ac subgrids connected through a bidirectional ac/dc converter known as IC. Coordinated control of ac and dc DERs in HMG is a challenging task due to the complexity of its structure and the distinct dynamics of dc and ac subgrids. In this article, a simple yet efficient decentralized control strategy was proposed to enable coordination of the DERs in ac and dc subgrids with fast dynamic response. The proposed method adopts piecewise linear V-I droop characteristics to enable accurate load sharing among the DERs within each subgrid. Compared with the conventional droop control methods (P-f, Q-V droop in ac and P-V droop in dc MGs), the V-I droop control method offers faster dynamics by removing the delays associated with

the calculation of average active and reactive powers. In addition, the V-I droop scheme enhances the power quality by elimination of the frequency deviation and decreasing the voltage deviations. A novel control method has been proposed for IC, in which the *d*-component of the ac bus voltage is adjusted as a function of the dc bus voltage and its derivative. The proposed control method eliminates the delays associated with PLL, which is commonly used in existing control schemes. Furthermore, by incorporating the derivative of the dc bus voltage in the control loop, the sluggishness caused by higher time constant of dc bus voltage (due large dc bus capacitors), is prevented. The efficacy of the proposed method has been verified through simulation and experimental results. The results show that in contrast with the conventional control method of HMG, which imposes the DERs to transient power overshoots, the proposed method realizes a smooth and overshoot-free response. In addition, the proposed method favors zero frequency deviations and tighter voltage regulation.

ACKNOWLEDGMENT

The authors would like to thank Prof. David J. Hill and the Smart Microgrid Research Laboratory of The University of Hong Kong, for providing support and assistance with regard to experimental implementation of the proposed control method.

REFERENCES

[1] P. C. Loh, D. Li, Y. K. Chai, and F. Blaabjerg, "Autonomous operation of hybrid microgrid with AC and DC subgrids," *IEEE Trans. Power Electron.*, vol. 28, no. 5, pp. 2214–2223, May 2013.

[2] L. Wang, X. Fu, and M.-C. W. Wong, "Operation and control of a hybrid coupled interlinking converter for hybrid AC/LVDC microgrids," *IEEE Trans. Ind. Electron.*, to be published.

[3] J. A. P. Lopes, C. L. Moreira, and A. G. Madureira, "Defining control strategies for microgrids islanded operation," *IEEE Trans. Power Syst.*, vol. 21, no. 2, pp. 916–924, May 2006.

[4] J. M. Guerrero, J. C. Vasquez, J. Matas, L. G. d. Vicuna, and M. Castilla, "Hierarchical control of droop-controlled AC and DC microgrids—A general approach toward standardization," *IEEE Trans. Ind. Electron.*, vol. 58, no. 1, pp. 158–172, Jan. 2011.

[5] X. Liu, P. Wang, and P. C. Loh, "A hybrid AC/DC microgrid and its coordination control," *IEEE Trans. Smart Grid*, vol. 2, no. 2, pp. 278–286, Jun. 2011.

[6] Z. Li and M. Shahidehpour, "Small-signal modeling and stability analysis of hybrid AC/DC microgrids," *IEEE Trans. Smart Grid*, vol. 10, no. 2, pp. 2080–2095, Mar. 2019.

[7] X. Shen, D. Tan, Z. Shuai, and A. Luo, "Control techniques for bidirectional interlinking converters in hybrid microgrids: Leveraging the advantages of both and dc," *IEEE Power Electron. Mag.*, vol. 6, no. 3, pp. 39–47, Sep. 2019.

[8] X. Li, Z. Li, L. Guo, J. Zhu, Y. Wang, and C. Wang, "Enhanced dynamic stability control for low-inertia hybrid AC/DC microgrid with distributed energy storage systems," *IEEE Access*, vol. 7, pp. 91234–91242, 2019.

[9] Y. Gu *et al.*, "Transfverter: Imbuing transformer-like properties in an interlink converter for robust control of a hybrid AC–DC microgrid," *IEEE Trans. Power Electron.*, vol. 34, no. 11, pp. 11332–11341, Nov. 2019.

[10] N. Eghtedarpour and E. Farjah, "Power control and management in a hybrid AC/DC microgrid," *IEEE Trans. Smart Grid*, vol. 5, no. 3, pp. 1494–1505, May 2014.

[11] Z. Liu, S. Miao, W. Wang, and D. Sun, "Comprehensive control scheme of the interlinking converter in hybrid AC/DC microgrid," *CSEE J. Power Energy Syst.*, to be published.

[12] L. He, Y. Li, J. M. Guerrero, and Y. Cao, "A comprehensive inertial control strategy for hybrid AC/DC microgrid with distributed generations," *IEEE Trans. Smart Grid*, vol. 11, no. 2, pp. 1737–1747, Mar. 2020.

[13] J.-W. Chang, S.-I. Moon, G.-S. Lee, and P.-I. Hwang, "A new local control method of interlinking converters to improve global power sharing in an islanded hybrid AC/DC microgrid," *IEEE Trans. Energy Convers.*, vol. 35, no. 2, pp. 1014–1025, Jun. 2020.

[14] Y. Xia, W. Wei, M. Yu, X. Wang, and Y. Peng, "Power management for a hybrid AC/DC microgrid with multiple subgrids," *IEEE Trans. Power Electron.*, vol. 33, no. 4, pp. 3520–3533, Apr. 2018.

[15] G. Qi, A. Chen, and J. Chen, "Improved control strategy of interlinking converters with synchronous generator characteristic in islanded hybrid AC/DC microgrid," *CPSS Trans. Power Electron. Appl.*, vol. 2, no. 2, pp. 149–158, 2017.

[16] G. Melath, S. Rangarajan, and V. Agarwal, "A novel control scheme for enhancing the transient performance of an islanded hybrid AC–DC microgrid," *IEEE Trans. Power Electron.*, vol. 34, no. 10, pp. 9644–9654, Oct. 2019.

[17] Z. Liu, S. Miao, Z. Fan, J. Liu, and Q. Tu, "Improved power flow control strategy of the hybrid AC/DC microgrid based on VSM," *IET Gener., Transmiss. Distrib.*, vol. 13, no. 1, pp. 81–91, 2018.

[18] A. A. Eajal, A. H. Yazdavar, E. F. El-Saadany, and M. M. Salama, "Optimizing the droop characteristics of AC/DC hybrid microgrids for precise power sharing," *IEEE Syst. J.*, to be published.

[19] M. S. Golsorkhi and D. D. C. Lu, "A control method for inverter-based islanded microgrids based on V-I droop characteristics," *IEEE Trans. Power Del.*, vol. 30, no. 3, pp. 1196–1204, Jun. 2015.

[20] M. S. Golsorkhi, R. Heydari, and M. Savaghebi, "An adaptive droop control method for interlink converter in hybrid AC/DC microgrids," in *Proc. 22nd Eur. Conf. Power Electron. Appl.*, 2020, pp. P.1–P.10.

[21] *IEEE Recommended Practice for Monitoring Electric Power Quality*, IEEE Standard 1159-2019 (Revision of IEEE Standard 1159-2009), 2019, pp. 1–98.

[22] M. S. Golsorkhi, D. D. Lu, and J. M. Guerrero, "A GPS-based decentralized control method for islanded microgrids," *IEEE Trans. Power Electron.*, vol. 32, no. 2, pp. 1615–1625, Feb. 2017.

[23] N. Pogaku, M. Prodanovic, and T. C. Green, "Modeling, analysis and testing of autonomous operation of an inverter-based microgrid," *IEEE Trans. Power Electron.*, vol. 22, no. 2, pp. 613–625, Mar. 2007.

[24] A. Yazdani and R. Iravani, *Voltage-Sourced Converters in Power Systems: Modeling, Control, and Applications*, Hoboken, NJ, USA: Wiley, 2010.

[25] J.-J. E. Slotine and W. Li, *Applied Nonlinear Control*. Hoboken, NJ, USA: Prentice hall Englewood Cliffs, 1991.

[26] A. Engler and N. Soultanis, "Droop control in LV-grids," in *Proc. Int. Conf. Future Power Syst.*, 2005, Art. no. 6.

Mohammad S. Golsorkhi received the B.Sc. (hons.) degree from Isfahan University of Technology, Isfahan, Iran, in 2009, the M.Sc. (hons.) degree from Tehran Poly Technique, Tehran, Iran, in 2012, and the Ph.D. degree from the University of Sydney, Sydney, NSW, Australia, in 2016, all in electrical engineering.

During 2015, he was a Visiting Ph.D. Student with the Department of Energy Technology, Aalborg University, Aalborg, Denmark. In 2016, he worked with The University of Hong Kong, Hong Kong as a Postdoctoral Fellow. Since 2017, he has been with the Department of Electrical and Computer Engineering, Isfahan University of Technology, Isfahan, Iran, where he is an Assistant Professor. His research interests include control of microgrids, multimicrogird systems, integration of renewable energy resources into distribution networks, and power electronics.

Mehdi Savaghebi (Senior Member, IEEE) received the B.Sc. degree from the University of Tehran, Tehran, Iran, in 2004, and the M.Sc. and Ph.D. degrees (with highest hons.) from Iran University of Science and Technology, Tehran, Iran, in 2006 and 2012, respectively, all in electrical engineering.

From 2014 to 2017, he was a Postdoc Fellow with the Department of Energy Technology, Aalborg University, Aalborg, Denmark, where he was an Associate Professor from 2017 to 2018. Currently, he is an Associate Professor and Research Team Leader with the Electrical Engineering Section, Department of Mechanical and Electrical Engineering, University of Southern Denmark, Odense, Denmark. His research interests include distributed generation systems, microgrids, power quality, and protection of electrical systems.

Dr. Savaghebi has been a Guest Editor of Special Issue on Power Quality in Smart Grids—IEEE TRANSACTIONS ON SMART GRID and Special Issue on Power Quality and Protection in Renewable Energy Systems and Microgrids—*IET Renewable Power Generation*. He is an Associate Editor of the IEEE ACCESS and a member of Technical Committee (TC) on Renewable Energy Systems and TC on Smart Grids, IEEE INDUSTRIAL ELECTRONICS SOCIETY.